ESR and ENDOR studies of holes trapped at cation vacancies in BeO†

B. Maffeo* and A. Hervé
Laboratoire de Résonance Magnétique, Centre d'Etudes Nucléaires de Grenoble, Cedex 85, 38041 Grenoble Gare, France
(Received 14 July 1975)

The V^- center (cation vacancy with a trapped hole) has been identified by ESR and electron-nuclear double resonance (ENDOR) in neutron- and electron-irradiated BeO crystals. At liquid-helium temperature, the defect is observed in two distinct configurations labeled "axial" and "nonaxial" where the hole is localized on an anion situated either along the $\vec{c}$ axis from the vacancy or on one of the three other corners of the tetrahedron, respectively. This model of an O^- ion next to a vacancy is supported by an analysis of the $\tilde{g}$ tensor. At room temperature, the hole jumps from one anion site to another around the vacancy, giving an isotropic averaged ESR spectrum. For the axial V^- center, ENDOR measurements were made at 1.5°K of the hyperfine interactions with the ^{9}Be nuclei which are nearest neighbors of the O^- ion and with two shells of next-nearest-neighbor nuclei. An analysis of the dipolar magnetic interaction with these nuclei gives detailed information about the electronic structure of the ground state of the defect and the lattice distortions in its vicinity. A comparison between the ENDOR spectra of the nonaxial V^- center and the V^0 center (cation vacancy with two trapped holes) confirms the close relation between these two defects. V^- centers associated with a trivalent impurity B^{3+} have been observed in γ-irradiated BeO crystals.

I. INTRODUCTION

The cation vacancy in the alkaline-earth oxides can trap a hole to form the so-called V^- center. The existence of this center was proposed for the first time by Wertz *et al.*[1] who identified its electron-spin-resonance (ESR) spectrum in MgO. The properties of this center have been reviewed in the articles on defects in oxides by Wertz and Henderson[2] and Henderson and Hughes.[3] In recent years, it has been the subject of numerous studies in MgO. In particular, the formation mechanism and the thermal stability have been studied by Abraham *et al.*[4] and Chen *et al.*[5] and by Tench and Duck.[6] Experiments combining ESR and magnetic circular dichroism have provided a positive correlation between the absorption band at 2.3 eV and the ESR spectrum.[7] A theory has been proposed by Schirmer *et al.*[8] to predict the line shape of the optical band in a model of a bound small polaron; this theory explains the position, the width, and the oscillator strength for the V^- center associated with a nearby impurity and the polarization of the absorption of the isolated V^- center when it is subjected to uniaxial stress. Rose and Cowan[9] have monitored the dichroism of the absorption induced by an external electric field and have deduced the electric dipole moment of the defect. ESR measurements of the alignment produced by uniaxial stress or an applied electric field have shown that the hole can tunnel around the vacancy from one oxygen to the next at liquid-helium temperature; the jump time has been determined by pulsed electron-electron double-resonance (ELDOR) experiments.[10] The thermally activated reorientation produces an isotropic ESR line at room temperature.[11] Schoenberg *et al.*[12] measured the hyperfine interaction with an ^{17}O nucleus for the V_1 center (V^- center with adjacent F^- ion). Halliburton *et al.*[11,13] analyzed the resolved hyperfine structure of the V^- center, due to the nucleus of an Mg^{2+} located next to the hole on the axis of the defect. These measurements provided definite evidence for the model of a highly localized hole. However, no complete study of interaction with the neighboring nuclei has yet been reported, owing to the difficulty of obtaining the ^{25}Mg ENDOR spectra. This is regrettable, for a study of the hyperfine interactions would provide a better understanding of the electronic structure of the defect.

Beryllium oxide is the first member of the alkaline-earth oxide series. As distinct from MgO, CaO, SrO which have the cubic NaCl structure, it has the hexagonal wurtzite structure. It possesses however a considerable advantage over these other oxides from the point of view of ESR and particularly ENDOR studies in that cation nuclei with spin (^{9}Be, $I = \frac{3}{2}$) are 100% abundant; in the other oxides mentioned, such nuclei have only small abundance.

In this paper, we present the results of an ESR and ENDOR study of the V^- center in BeO. We analyze the magnetic hyperfine interactions with three different shells of beryllium neighbors. This provides us with detailed information about the electronic and geometric structure of the defect. Finally, in Secs. V and VI, we will present

results concerning the V^0 center (cation vacancy with two trapped holes) and the V_B center (cation vacancy associated with a trivalent boron impurity). Part of this work has already been described in several preliminary publications.[14,15]

II. EXPERIMENTAL

The BeO crystals used in this work were supplied by Dr. S. B. Austermann (Autonetics Division, North American Rockwell). They were hexagonal prisms of about 20mm^3 volume, with the longest dimension parallel to the $\vec{c}$ axis. They were placed in the microwave cavity with either the (0001) or a $(1\bar{2}10)$ plane horizontal; the orientation could be corrected to within $\frac{1}{4}^\circ$ by tilting the cavity while observing the crossings of the V^0 center ESR lines when $\vec{H}_0$ is applied along crystallographic axes.

The crystals were irradiated with fast particles in a nuclear reactor or on an electron accelerator at ambient temperature at the Centre d'Etudes Nucléaires de Grenoble. The integrated doses were 10^{18} cm^{-2} for neutrons (of energies >1 MeV) and 10^{19} cm^{-2} for the electron irradiations, which were at 3 MeV. The ESR measurements were performed at room temperature, at 4.2 °K and at 1.5 °K, using a Varian 4520 model spectrometer operating at Q band (35 GHz) with 100-kHz field modulation.

The ENDOR measurements were all performed at 1.5 °K, using a cylindrical TE_{011} cavity whose construction has been described by Santier.[16] The helicoidal metallic body of this cavity is transparent to the 100-kHz field modulation and acts as the radiofrequency coil; this coil is placed in series with coaxial cables terminating in a 50-Ω matched load. The input cable is connected to a wide band Instruments for Industry model 5000 amplifier (30-dB gain) driven by a Ferisol model LF101B 1-mW rf generator. A rf magnetic field of about 1 G is obtained at the sample with this arrangement. The output of the generator is frequency modulated at 80 Hz to a depth of 1–8 kHz dependent on the width of the ENDOR line. Detection of the frequency-modulated signal eliminates noise due to instability of magnetic field, etc., giving a very flat baseline; the spectrum trace is then the first derivative of the ENDOR spectrum.

III. ESR OF V^- CENTER

In Fig. 1, we give the ESR spectrum taken at 1.5 °K for a BeO crystal which had been irradiated with 3-MeV electrons. The magnetic field $\vec{H}_0$ is parallel to the $\vec{c}$ axis of the crystal. The figure shows only the region around $H_0 = 13\,250$ G (resonant field of the free electron).

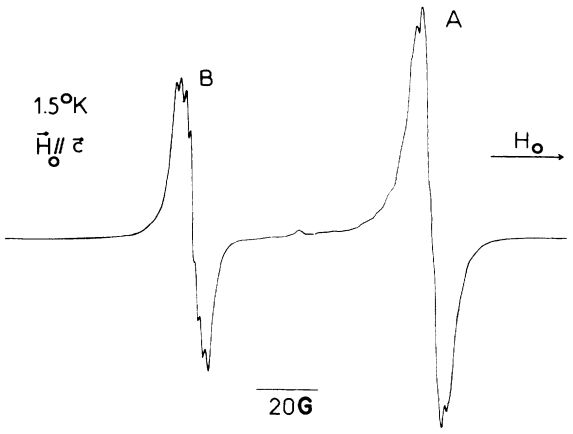

FIG. 1. 1.5 °K Q-band ESR spectrum of the V^- center in a BeO crystal which had been irradiated with 3-MeV electrons. $\vec{H}_0$ is parallel to the $\vec{c}$ axis. Lines A and B correspond to the axial and nonaxial configurations, respectively.

For this orientation, the spectrum is made up of two lines separated by 76 G, each line having a partially resolved hyperfine structure [the ESR line of the F^+ center[17,18] occurs in the same region of the spectrum but is invisible, being strongly saturated at the microwave power levels used in the present study].

The line designated A at $g = 2.0026$ is more intense than the other line B at $g = 2.0149$. The structure of line A changes when the orientation

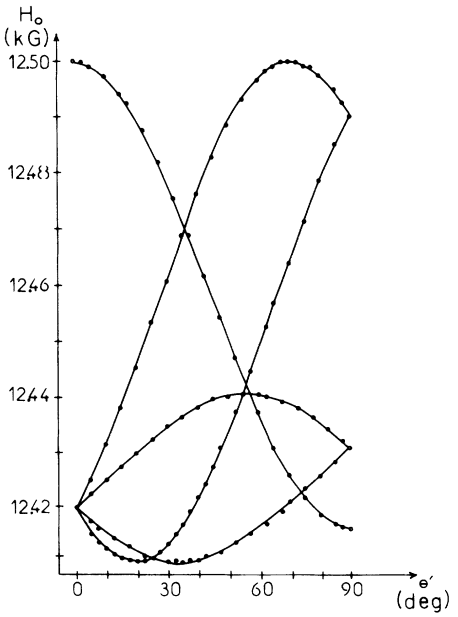

FIG. 2. Variation of the positions of the V^--center ESR lines when $\vec{H}_0$ rotates in a $(1\bar{2}10)$ plane. θ' is the angle between $\vec{H}_0$ and the $\vec{c}$ axis.

of the magnetic field is changed but this line does not split. Line B splits into six equal intensity components when the magnetic field is turned to an arbitrary orientation. Figures 2 and 3 show the angular variation of the ESR spectrum when the magnetic field is rotated in a mirror plane $(1\bar{2}10)$ and in the plane perpendicular to $\vec{c}$, (0001). For the $(1\bar{2}10)$ plane, line B splits into four lines of relative intensities 2-2-1-1. For the plane perpendicular to $\vec{c}$, it splits into three equally intense lines. The angular variation is very well described with a spin Hamiltonian

$$\mathcal{H} = \mu_B \vec{H}_0 \cdot \vec{\vec{g}} \cdot \vec{S} \quad (\mu_B, \text{ Bohr magneton}), \qquad (1)$$

where $S = \frac{1}{2}$ and $\vec{\vec{g}}$ is a cylindrical tensor.

For line A, the principal axis of the $\vec{\vec{g}}$ tensor is parallel to $\vec{c}$ and the principal values are $g_{\parallel} = 2.0026 \pm 0.0005$, $g_{\perp} = 2.0155 \pm 0.0005$. We will designate by the term "axial" the defect corresponding to this line.

For lines B, the principal axis of the $\vec{\vec{g}}$ tensor lies in a $(1\bar{2}10)$ symmetry plane of the crystal and is parallel to one of the nonaxial Be-O directions (there are six such directions because there are two types of tetrahedron in the wurtzite structure). We will term the corresponding defect the "nonaxial" defect. The $\vec{\vec{g}}$ tensor has principal values $g_{\parallel} = 2.0026 \pm 0.0005$ and $g_{\perp} = 2.0164 \pm 0.0005$.

These results show that line A corresponds to a paramagnetic center having C_{3v} symmetry. Line B corresponds to a center having C_s symmetry (the measurement precision is not sufficient to determine the deviation of the $\vec{\vec{g}}$ tensor from cylindrical symmetry, however). These symmetry properties are verified by the ENDOR observations (Sec. IV), which provide a very precise test of the symmetry of the defect's environment.

We attribute the A and B spectra to a V^- center, a lattice defect consisting of an *isolated* beryllium vacancy which has trapped a hole. At liquid-helium temperature, the hole is effectively localised on a single anion, thus forming an O^- ion. As a result of the polar field of the wurtzite lattice, there are two slightly different types of V^- center, namely (A) the axial defect where the vacancy-hole direction is parallel to $\vec{c}$ and (B) the nonaxial defect, where the vacancy-hole direction corresponds to one of the three Be-O bonds inclined at 109° to the $\vec{c}$ axis. There are two axial sites and six nonaxial sites because the wurtzite lattice, a portion of which is shown in Fig. 4, contains two types of oxygen tetrahedra related by a rotation of 180° around $\vec{c}$. The two possible configurations of the beryllium ions surrounding the O^- ion are shown in Fig. 5: the O^- ion is situated at the center of a tetrahedron of cations in which one of the corners is unoccupied (the corner in the $\vec{c}$ axis direction in the axial defect, one of the corners in the basal

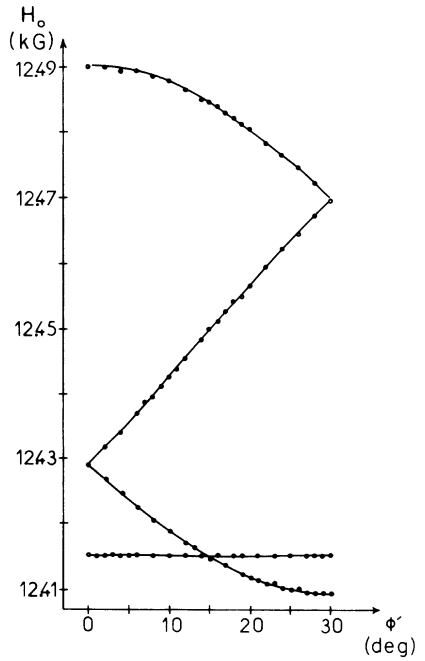

FIG. 3. Variation of the positions of the V^--center ESR lines when $\vec{H}_0$ rotates in the (0001) plane. ϕ' is the angle between $\vec{H}_0$ and a $\langle 0\bar{1}10 \rangle$ direction.

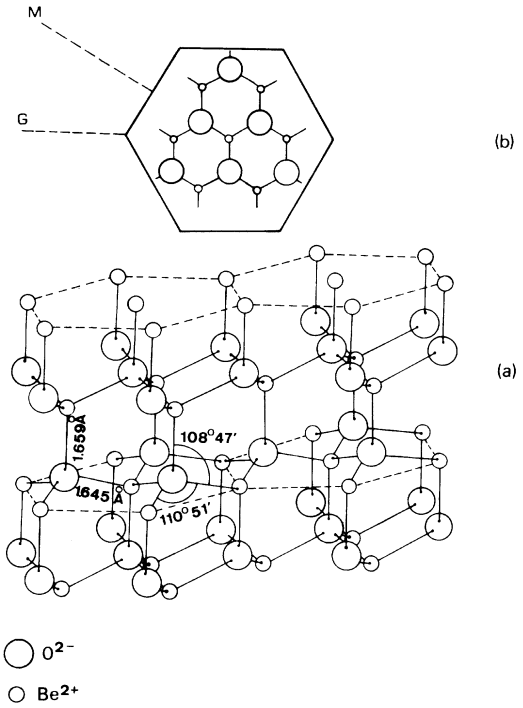

FIG. 4. Portion of the hexagonal crystal structure of BeO.

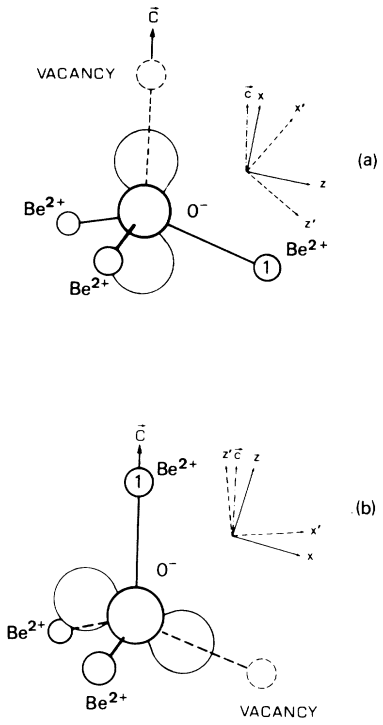

FIG. 5. Model of the V^- center showing the orientation of the p orbital in the O^- ion and the disposition of the nearest neighbors of this ion in (a) the axial and (b) the nonaxial configuration. The plane of the figure is the vacancy-O^--Be^{2+}(1) plane. The axis x and z (x' and z') lie in this plane, being principal directions of the $\vec{\vec{A}}(\vec{\vec{Q}})$ tensor.

plane of the tetrahedron in the nonaxial defect). In Fig. 5, the ion have been placed at the positions corresponding to the undistorted lattice.

From this model, one can obtain a qualitative explanation of the properties of the $\vec{\vec{g}}$ tensor. The electric field of the vacancy lifts the orbital degeneracy of the ^2P ground term of the O^- ion (which is the only term of the ground configuration $1s^2 2s^2 2p^5$). The ground state is then a nondegenerate state ^2P_z in which the unpaired electron occupies an orbital whose axis is parallel to the O^--ion–vacancy direction. If one assumes that the spin-orbit coupling is weak compared to the energy differences between the p_z and the p_x, p_y orbitals, a simplified calculation of the principal values of the $\vec{\vec{g}}$ tensor can be performed using perturbation theory. The $\vec{\vec{g}}$ tensor then has cylindrical symmetry around the axis of the p_z orbital and its principal values are

$$g_{\parallel} = g_e \ , \quad g_{\perp} = g_e(1 - \lambda/\Delta E), \tag{2}$$

where g_e is the g factor of the free electron (2.0023), λ is the spin-orbit coupling constant for the O^- ion (which is negative), and ΔE is the (positive) energy difference between the p_z orbital and the p_x, p_y orbitals.

The predictions of this calculations, in particular that $\Delta g_{\perp} > 0$, are in qualitative agreement with our experimental results. Of course, in the nonaxial defect, p_x and p_y do not have exactly equal energy and the $\vec{\vec{g}}$ tensor should be orthorhombic, but the energy separation between these two orbitals is apparently too small to create a detectable effect. We will postpone further discussion of the $\vec{\vec{g}}$ tensors, leaving for Sec. IV an estimate of the value of ΔE.

Owing to the effect of the polar field of the crystal, the axial and nonaxial configurations of the trapped hole defect have slightly different energies. In Fig. 1, we see that line A is more intense than line B, instead of having $\frac{1}{3}$ of its intensity, showing that the axial configuration is preferentially populated. However, the energy difference between the two sites does not exceed a few degrees Kelvin.

Thus, in the proposed model, the axial and nonaxial defects correspond to the different equilibrium configurations of the −1 charge state of the isolated cation vacancy, which lowers its energy by a strong trigonal distortion. At liquid-helium temperature, the hole spends a sufficiently long time on a given site so that one can observe the ESR spectrum of the defect frozen in a particular distorted configuration. One might expect that the lattice vibrations would cause the hole to jump from site to site around the vacancy at sufficiently high temperature, which would have the following effect on the ESR spectrum. For very high jump frequencies (much greater than the difference between the resonance frequencies of the different sites) a single ESR line should be observed at a g value $\bar{g}$ equal to the mean of the g factors of the four different sites (at high temperature, the population difference between the axial and nonaxial configurations is negligible). From the low-temperature g values, we calculate that the position of the averaged line should be practically independent of the orientation of $\vec{H}_0$, lying at $g = 2.0117 \pm 0.0005$. This averaged line would not be expected to have resolved hyperfine structure because the hole would interact with 12 nearest-neighbor beryllium nuclei.

Figure 6 shows the 300 °K ESR spectrum of a (neutron irradiated) BeO crystal for $\vec{H}_0$ parallel to $\vec{c}$. The V^- center lines observed at liquid-helium temperature do not appear. The spectrum consists instead of two lines. One of these, situated at $g = 2.0035 \pm 0.0002$ has partially resolved hyperfine structure; it corresponds to the F^+ center. The other line has a slightly asymmetric line

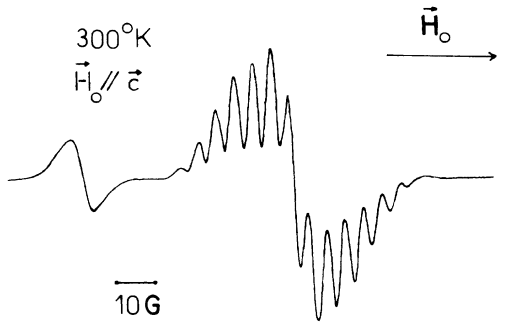

FIG. 6. Room-temperature Q-band ESR spectrum of neutron-irradiated BeO, with $\vec{H}_0$ parallel to $\vec{c}$. The structured line corresponds to the F^+ center. The line without structure is the averaged spectrum of the V center.

shape and no resolved structure. Its g value is isotropic and equal to 2.0118 ± 0.0001. We attribute this line to the averaged spectrum of the V^- center. Its width is minimum (4 G) when $\vec{H}_0$ is orientated such that is makes equal angles with the four Be-O directions in one of the two tetrahedra of the lattice. The anisotropy of the linewidth shows that the averaging effect is not complete at room temperature; the jump frequency at this temperature is of order 10^{10} sec^{-1}. We note that the V^- center spectrum is stable for anneals up to 200 °C so that this defect provides an example of a physical system for which the reorientation behavior could be studied over a wide range of temperatures and frequencies.

Thus, the trapped hole model gives a good interpretation of the liquid-helium and room temperature ESR spectra. The ENDOR measurements described in the next section will enable us to deduce the electronic and geometric structure of the defect much more precisely.

IV. ENDOR OF AXIAL V^- CENTER

A. Results

1. Nearest-neighbor nuclei

Figure 7 shows the ENDOR spectrum which is obtained by saturating the ESR line of the axial V^- center for $\vec{H}_0$ parallel to $\vec{c}$. The spectrum is centered approximately on the resonant frequency $\nu = 7.45$ MHz of the free beryllium nucleus in the applied field $\vec{H}_0$, which unambiguously identifies the nuclei involved in the hyperfine interactions.

The two three line patterns centered at 5.1 and 9.9 MHz, respectively, are attributed to the three beryllium nuclei which are nearest neighbors to the O^- ion; these nuclei lie in the three $(1\bar{2}10)$ symmetry planes of the defect [see Figs. 4 and 5(a)]. They are equivalent for this orientation of the magnetic field and the threefold splitting of the ENDOR transition is due to the quadrupole interaction with the electric field gradient at the nucleus. When $\vec{H}_0$ makes an angle $\theta' \neq 0°$ with $\vec{c}$ within a $(1\bar{2}10)$ plane, two nuclei for each kind of center are magnetically inequivalent and one observes four sets of quadrupole split triplets (see Fig. 8). When $\vec{H}_0$ rotates in the (0001) plane, making an angle ϕ' with a $\langle 0\bar{1}10 \rangle$ direction, the spectra of the two defect sites are indistinguishable and only three inequivalent nuclei are observed (see Fig. 9).

The interaction of the defect with a given nucleus is described by the spin Hamiltonian

$$\mathcal{H}_0 = \mu_B \vec{H}_0 \cdot \vec{\bar{g}} \cdot \vec{S} - g_n \mu_N \vec{H}_0 \cdot \vec{I} + \vec{I} \cdot \vec{\bar{A}} \cdot \vec{S} + \vec{I} \cdot \vec{\bar{Q}} \cdot \vec{I}, \tag{3}$$

where $I = \frac{3}{2}$ is the nuclear spin ($\vec{\bar{Q}}$ is the electric quadrupole interaction tensor). The angular variation shown in Fig. 8 is for a symmetry plane of the defect and therefore for a principal plane of the tensors $\vec{\bar{A}}$ and $\vec{\bar{Q}}$ associated with the two beryllium nuclei (one for each site) belonging to the plane of the variation. The upper ENDOR lines of these nuclei are indicated by a and a' in Fig. 8. Their frequencies are given by

$$\nu(m_s, m_q) = \{\nu_L^2 - 2m_s\nu_L[(A_x - A_z)\sin^2\alpha + A_z]/h + m_s^2[(A_x^2 - A_z^2)\sin^2\alpha + A_z^2]/h^2\}^{1/2} + m_q W_q/h, \tag{4}$$

$\vec{x}$ and $\vec{z}$ are the principal axes of the tensor $\vec{\bar{A}}$ in the plane of variation of $\vec{H}_0$, ν_L is the Larmor frequency of the free beryllium nucleus and, α is the angle between $\vec{H}_0$ and $\vec{z}$. The quantity W_Q is

$$W_Q = 3(Q_{z'} - Q_{x'})\cos^2\gamma + Q_{x'}, \tag{5}$$

where $\vec{x}', \vec{z}'$ are the principal axes for the tensor $\vec{\bar{Q}}$ in this phane, γ is the angle between $\vec{H}_0$ and the quantisation axis of the nuclear spin, $m_q = \frac{1}{2}(m_I + m_I')$ where m_I and m_I' are the quantum numbers associated with the levels linked by the ENDOR transition (for $I = \frac{3}{2}$, $m_q = 1, 0,$ or -1).

When $\vec{H}_0$ is perpendicular to a $(1\bar{2}10)$ plane, it is parallel to $\vec{y}$, the common axis of the tensors $\vec{\bar{A}}$ and $\vec{\bar{Q}}$ of the two nuclei situated in this plane. The ENDOR frequencies are simply given by

$$\nu(m_s, m_q) = \nu_L - m_s A_y/h + m_q 3Q_y/h. \tag{6}$$

The parameters defining the tensors $\vec{\bar{A}}$ and $\vec{\bar{Q}}$ were obtained from the angular variations of Figs. 8 and 9 by applying formulas (4)–(6). The results are given in Table I.

The magnetic interaction tensor $\vec{\bar{A}}$ is approximately cylindrical around a direction which makes an angle of about 10° with a "nonaxial" Be-O direction of the perfect crystal. The form of the

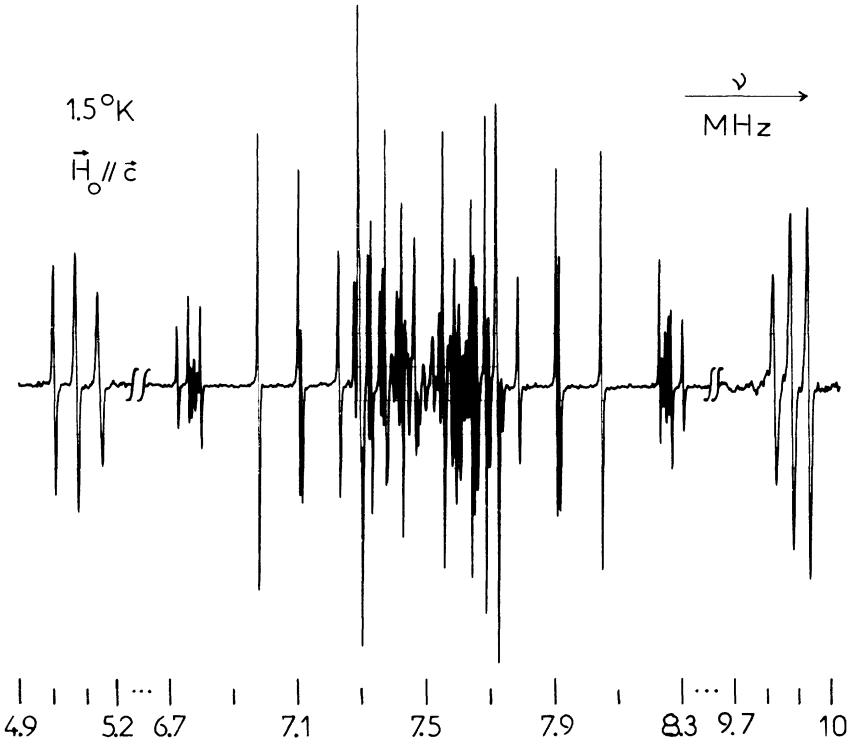

FIG. 7. 1.5 °K ENDOR spectrum of the axial V^- center for $\vec{H}_0$ parallel to $\vec{c}$.

angular variations shows that the three principal values of the $\bar{A}$ tensor have the same sign: the absolute signs given in the table are deduced from a theoretical discussion based on the model of the defect (Sec. IV B). Knowing this sign, we could determine the signs of the quadrupole constants experimentally by selectively saturating the different hyperfine components of the ESR line and observing the corresponding variations in the intensities of the different lines of the quadrupole triplet; the signs given in the table were obtained in this way.

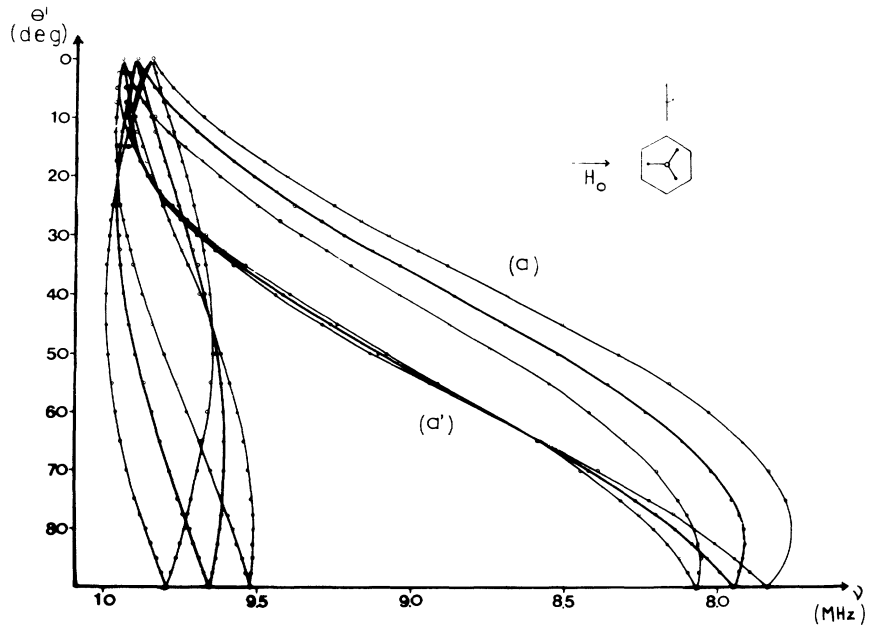

FIG. 8. Variation of the position of the high-frequency ENDOR lines for the beryllium nuclei which are nearest neighbors to the O^- ion in the axial V^- center. $\vec{H}_0$ is in a $(1\bar{2}10)$ plane, making an angle θ' with the $\vec{c}$ axis.

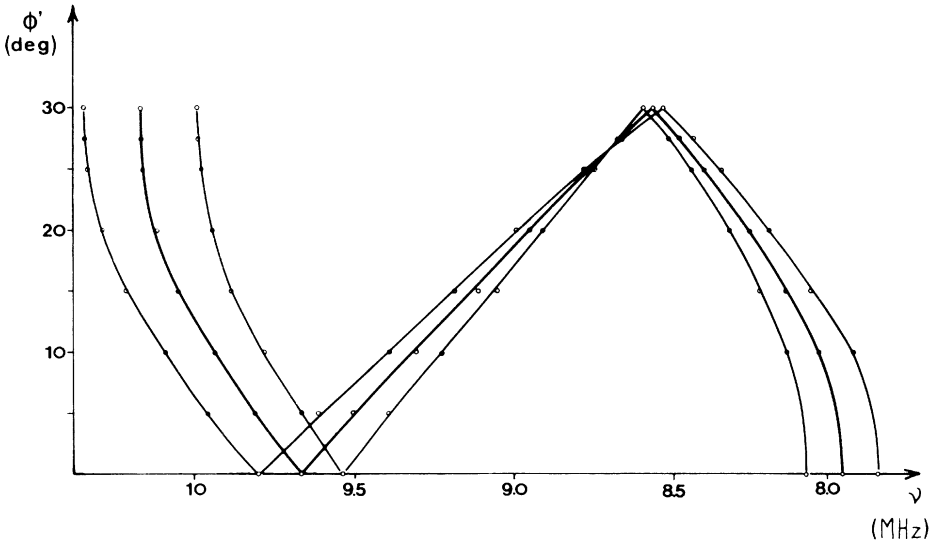

FIG. 9. Variation of the same ENDOR lines as in Fig. 8 when $\vec{H}_0$ rotates in the (0001) plane, making an angle ϕ' with a $\langle 0\bar{1}10\rangle$ direction.

If $a = \frac{1}{3}(A_x + A_y + A_z)$ is the isotropic part of the tensor $\bar{A}$, $b = \frac{1}{2}(A_z - a)$ is the cylindrical part and $b' = \frac{1}{2}(A_x - A_y)$ is a measure of the deviation from cylindrical symmetry, we obtain the following values from Table I:

$a = 3.667$ MHz, $b = -1.506$ MHz,

$b' = -0.319$ MHz

(it is important to remark that $g_n < 0$ for the ^{9}Be nucleus).

2. *Next-nearest-neighbor nuclei*

The central part of the spectrum between 6.6 and 8.4 MHz corresponds to second- and more-distant-neighbor nuclei for both the V^- center and the F^+ center; (Garrison and DuVarney[19] have studied the ENDOR transitions of the second neighbors of the F^+ center). Despite the very small line width (less than a kHz in some cases), the analysis of the V^- center spectrum is made extremely difficult by the huge number of transitions which are crowded into a narrow frequency range for orientations of $\vec{H}_0$ not parallel to $\vec{c}$. The line positions were measured every half degree of angle as $\vec{H}_0$ was rotated in a $(1\bar{2}10)$ plane and in the (0001) plane. Two types of nuclei which are next-nearest neighbors to the O^- ion could be identified.

The first type consists of only a single nucleus, which is situated along the $\vec{c}$ axis from the O^- ion, in the opposite direction from the vacancy (see Fig. 4). The second identifiable group consists of three nuclei situated in the same (0001) plane as the first-neighbor nuclei (see Fig. 4). We will term the first nucleus the "axial" next-nearest-neighbor (nnn) nucleus and the second "nuclei" the lateral next-nearest-neighbir (nnn) nuclei (the same labels are used for the F^+ center case by Garrison and DuVarney[19]).

For $\vec{H}_0$ parallel to $\vec{c}$, the spectrum of the axial nnn nucleus consists of two quadrupole triplets centered at 6.8 and 8.3 MHz, respectively; they are designated b in Figs. 10 and 11. The tensors $\bar{A}$ and $\bar{Q}$ for this nucleus have accurately cylindrical symmetry around $\vec{c}$. The principal values are given in Table I. The magnetic constants deduced

TABLE I. Hyperfine constants (unit: MHz) for the nearest-neighbor (nn) and next-nearest-neighbor (nnn) beryllium nuclei in the axial V^- center. The angles τ and τ' are the angles between the $\vec{c}$ axis and the axes $\vec{z}$ and $\vec{z}'$ of the tensor $\bar{A}$ and $\bar{Q}$, respectively.

Nucleus	A_z/h	A_x/h	A_y/h	$Q_{z'}/h$	$Q_{x'}/h$	$Q_{y'}/h$	τ	τ'
nn	+0.655	+4.855	+5.492	−0.071	+0.007	+0.064	98.5°	125°
	±0.005	±0.005	±0.005	±0.001	±0.001	±0.001	±0.5°	±1°
axial nnn	−1.472	+0.313	+0.313	±0.004	∓0.002	±0.002	0°	0°
	±0.002	±0.002	±0.002	±0.0004	±0.0004	±0.0004		
lateral nnn	−0.580	+0.273	+0.319	±0.017	∓0.0045	∓0.013	95°	0°
	±0.002	±0.006	±0.004	±0.003	±0.0005	±0.002	±0.5°	±0.5°

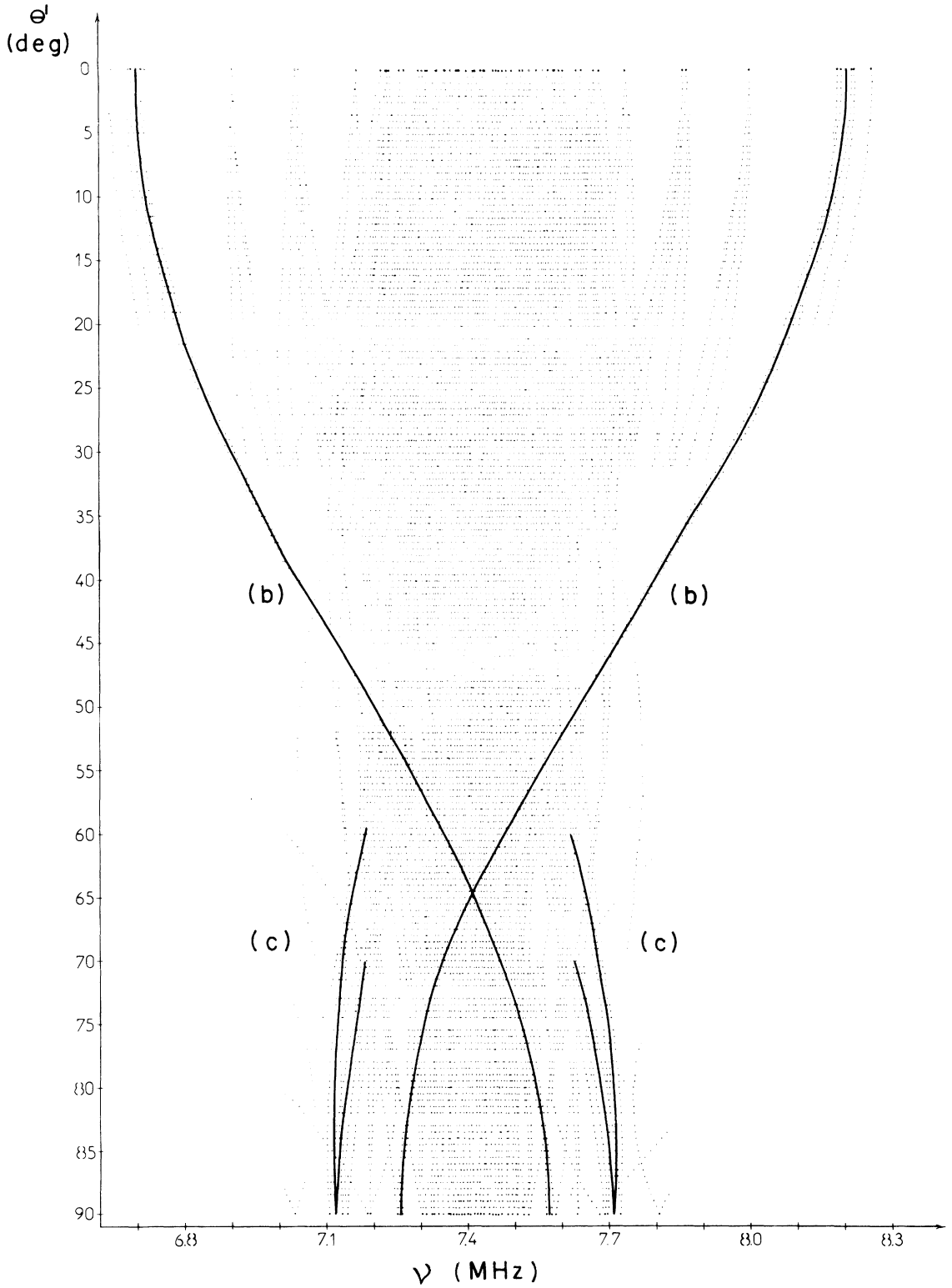

FIG. 10. Variation of the central region of the axial V^- center's ENDOR spectrum when $\vec{H}_0$ rotates in a $(1\bar{2}10)$ plane, making an angle θ' with $\vec{c}$. The curves (experimental and fitted) trace the variation of the central line of the quadrupole triplet for: (i) the axial [lines labelled (b)] and (ii) the lateral [lines labelled (c)] next-nearest-neighbor beryllium nuclei. Only the part that was used in the fitting is indicated.

from the values of the tensor $\vec{\vec{A}}$ are

$a = -0.282 \pm 0.002$ MHz,

$b = -0.595 \pm 0.002$ MHz.

Owing to the complexity of the central region of the spectrum, the lines corresponding to the lateral nnn nuclei could not be identified unambiguously for $\vec{H}_0$ parallel to $\vec{c}$. One of the reasons for this complexity can be seen in the region $0^\circ \leq \theta' \leq 35^\circ$ of Fig. 10; in this angular interval we saturate simultaneously the axial V^- and F^+ centers ESR lines so that the ENDOR lines associated with the latter center appear also.

When $\vec{H}_0$ is perpendicular to $\vec{c}$ in a $(1\bar{2}10)$ plane, one observes two quadrupole triplets (designated c in Figs. 10 and 11) at either side of the free beryllium Larmor frequency. When $\vec{H}_0$ is displaced away from this direction within the $(1\bar{2}10)$ plane, each line splits into two so that there are two sets of two quadrupole split triplets; their variation could be studied over a limited range of angles (see Fig. 10). There is no line doubling when $\vec{H}_0$ is rotated in the plane perpendicular to $\vec{c}$. Thus, each set can be associated with one beryllium nucleus situated in the particular $(1\bar{2}10)$ symmetry plane of the defect chosen for the angular variation, the two sets corresponding to the two defect sites. These symmetry properties show that this nucleus, like the nearest-neighbor nucleus discussed in Sec. IV A 1, belongs to a shell of three nuclei which are equivalent when $\vec{H}_0$ is parallel to $\vec{c}$.

The principal values and principal directions of the $\vec{\vec{A}}$ and $\vec{\vec{Q}}$ tensors were deduced from a combination of direct measurements and curve fitting using the least-squares method. The results are given in Table I. From these results we deduce

$a = 0.004 \pm 0.004$ MHz, $b = -0.292 \pm 0.004$ MHz,

$b' = -0.023 \pm 0.005$ MHz.

The measured values of the $\vec{\vec{A}}$ tensor show that the ENDOR lines of the other nuclei of the same shell must lie in the region closer to the free beryllium Larmor frequency. These lines could not be identified with certainty.

The magnetic hyperfine interaction is almost cylindrical around an axis $\vec{z}$ making an angle 95° with the $\vec{c}$ axis. In the perfect crystal, the direction joining the anion site to the lateral next-nearest-neighbor (nnn) Be^{2+} nucleus makes an angle 99.7° with the $\vec{c}$ axis. This fact and the above symmetry properties enable us to identify the nucleus giving rise to the ENDOR lines labelled c in Fig. 8 with the lateral next-nearest-neighbor beryllium.

B. Discussion of ENDOR results

1. Theory of anisotropy parameters b and b'

a. Case of a pure p orbital. We have seen that in the simplest model of the electronic structure of the axial defect, the crystal field lifts the degeneracy of the ^2P ground term of the O^- ion and the unpaired electron occupies a pure $2p_z$ orbital which is parallel to the $\vec{c}$ axis. In this model, one can readily estimate the parameters b and b' for the first and second-neighbor beryllium nuclei.

We designate the distance between the O^- ion nucleus and the beryllium nucleus by v and the angle between the O^- – Be direction and the $\vec{c}$ axis by τ. The index 1 will refer to the nearest-neighbor nucleus, the index 2 to the axial nnn nucleus and the index 3 to the lateral nnn nucleus. The distances and angles for these nuclei in the perfect crystal are indicated in Fig. 12.

We will assume that the measured hyperfine axis

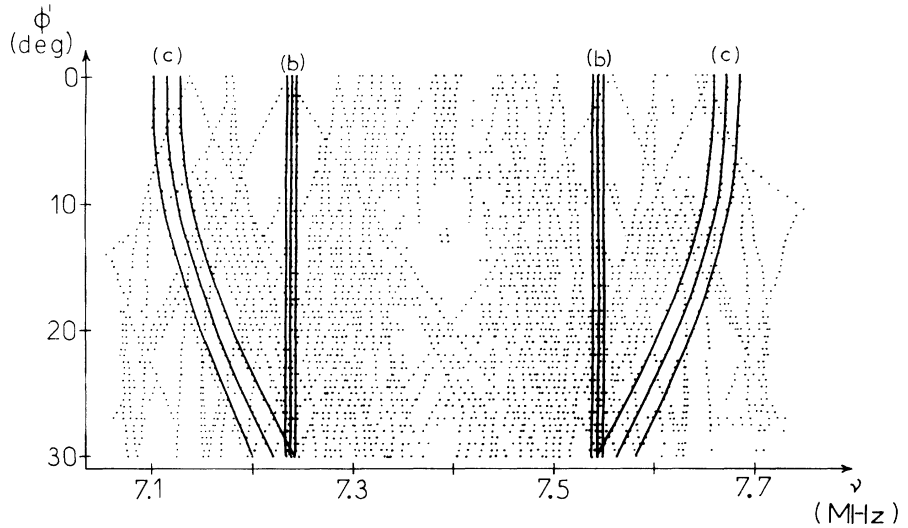

FIG. 11. Variation of the central region of the axial V^- center's ENDOR spectrum when $\vec{H}_0$ rotates in the (0001) plane, making an angle ϕ' with a $\langle 0\bar{1}10 \rangle$ direction. Experimental and fitted curves (b) and (c) correspond to the axial and lateral next-nearest-neighbor nuclei, respectively.

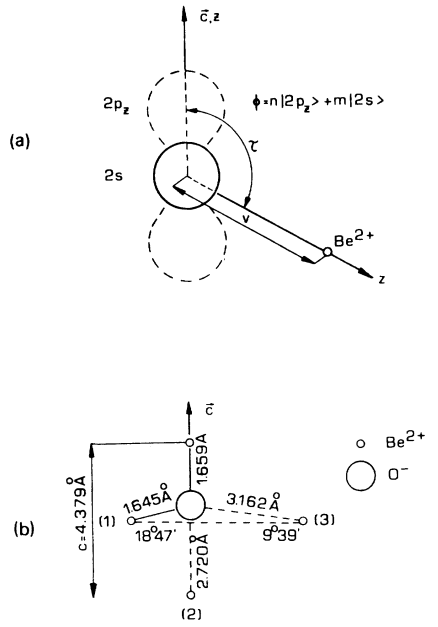

FIG. 12. Model used in the discussion of the anisotropic hyperfine interactions of the axial V^- center, showing the relative orientations of the directions joining the O^- ion nucleus to the nearest- and next-nearest-neighbor beryllium nuclei.

corresponds to the line joining the O^- ion to the Be nucleus in the defect: this will be seen to be justified approximately. We further neglect the displacement of the lateral nnn nucleus with respect to its position in the perfect crystal. The following important result then follows from the experimental hyperfine interactions: the O^- ion is displaced from the normal anion site, approaching the plane of the nearest-neighbor beryllium ions. This result indicates that the O^- ion is repelled by the negatively charged vacancy, as one would expect. By taking the experimental value τ_z measured for nucleus 3, we estimate that the O^- ion lies about 0.28 Å above the plane of the nearest-neighbor beryllium nuclei [instead of 0.55 Å in the perfect crystal; see Figs. 4 and 5(a)].

The constants b and b' can be written

$$b = \tfrac{1}{2} g_e g_n \mu_B \mu_N \langle p_z | (3z^2 - r^2)/r^5 | p_z \rangle, \quad (7)$$

$$b' = \tfrac{3}{2} g_e g_n \mu_B \mu_N \langle p_z | (x^2 - y^2)/r^5 | p_z \rangle \quad (8)$$

(μ_N: nuclear magneton; g_n: g factor of the Be nucleus), where r is the electron-nucleus distance and xyz is the principal-axis system for the particular nucleus. To carry out the necessary integrations, it is convenient to take a new origin at the centre of the p orbital and to introduce a new variable $\vec{\rho} = \vec{r} - \vec{v}$, where $\vec{\rho}$ is the vector defining the position of the electron with respect to this new origin; the functions to be averaged are then expanded in ρ/v. This gives

$$b = g_e g_n \mu_B \mu_N (1/v^3)[1 + \tfrac{6}{5}(3\cos^2\tau - 1)\langle \rho^2 \rangle / v^2], \quad (9)$$

$$b' = g_e g_N \tfrac{3}{5} \sin^2\tau \langle \rho^2 \rangle v^5. \quad (10)$$

Here,

$$\langle \rho^2 \rangle = \int_0^\infty \rho^2 |R_{2p}(\rho)|^2 \rho^2 d\rho,$$

where $R_{2p}(\rho)$ is the radial part of the $2p_z$ orbital.

From the experimental values of b_1 and b_1', we calculate that for the first-neighbor nucleus, $v_1 = 1.72$ Å and $\langle \rho^2 \rangle = 0.75 \pm 0.02$ Å^2. Then, for nucleus 3, using the measured value of b and this value of $\langle \rho^2 \rangle$, we obtain $v_3 = 3.15 \pm 0.02$ Å and $b_3' = -16 \pm 1$ kHz; the latter figure is to be compared with the measured value -23 ± 5 kHz.

The results obtained for these two nuclei appear very satisfactory. The distance 1.72 Å derived for nucleus 1 is somewhat longer than the distance from the normal position of this nucleus to the relaxed position (derived earlier) of the O^- ion; this indicates that there is an outward relaxation of nucleus 1 under the action of the charge-defect situated on the O^- ion. The distance 3.15 Å determined for nucleus 3 is equal, within the experimental error, to the calculated distance from the relaxed position of the O^- ion to the normal lattice position of this nucleus.

The value determined for $\langle \rho^2 \rangle$ is slightly smaller than the value 0.85 Å^2 calculated from Clementi's Hartree-Fock wave functions[20] for O^-. The decrease in $\langle \rho^2 \rangle$ in the crystal as compared with the free ion value can be explained by the Pauli exclusion principle and the electrostatic interactions between electrons belonging to different ions. These effects tend to concentrate the electronic density around the nuclei, as is shown by the calculation of Gourary and Adrian[21] for the orbital of the unpaired electron in the F center in Li F.

We now analyze the results obtained for the axial nucleus, number 2. If this nucleus is assumed to be fixed, the relation of the O^- ion along the $\vec{c}$ axis places it at 2.47-Å distance. By using $\langle \rho^2 \rangle = 0.75$ Å^2, one obtains $b_2 = 970$ kHz, which is in very marked disagreement with the experimental value 595 kHz. In the following, we will discuss various possible explanations for this disagreement. We first discuss two approximations we have made.

First, we have neglected the second-order contributions to the spin-nucleus dipolar interaction as well as the interaction between the nucleus and the orbital angular momentum of the electron[22]; however, these corrections can be shown to be of

order 1% only ($\Delta g_\perp$ is very small). Second, to take into account the Pauli principle, we should use a wave function which is orthogonalised to the Be^{2+} ion cores. The $2p_z$ wave function is already practically orthogonal to the $1s$ functions on the laterally situated Be^{2+} ion (1 and 3) since these lie almost in its equatorial plane. However, for the axial Be^{2+} ion, there is a small overlap $S=\langle 1s(Be^{2+})|2p_z(O^-)\rangle$, which introduces a correction term of order

$$-2Sg_e g_n \mu_B \mu_N \langle 1s|(3z^2-r^2)/r^5|2p_z\rangle.$$

This term also can only slightly reduce the disagreement.

Another mechanism which could reduce the value of b_2 is a partial delocalization of the hole onto the three other anions O^{2-} which surround the vacancy. This delocalisation can be understood as follows. Consider first a symmetric configuration of the four oxygen nuclei of the vacant tetrahedron. The $2p$ orbitals directed towards the vacancy form basis states for A_1 and T_2 irreducible representations of the T_d symmetry point group of the tetrahedron (we neglect the small polar field of the crystal). In the negative charge state of the vacancy, the hole would presumably occupy the T_2 level, which has highest energy; however, the vacancy undergoes a trigonal distortion owing to a strong static pseudo-Jahn-Teller effect which mixes the different orbitals together. In the distorted state, the hole wave function, concentrated mainly on one oxygen, will be a linear combination of the $2p$ orbitals of all the oxygens, with coefficients which depend on the mixture of the A_1 and T_2 orbitals. An upper limit on the possible degree of delocalisation of the hole onto the other three anions can be deduced from the principal values of the $\tilde{g}$ tensor. If P is the probalility of finding the hole on one of these three anions, the value of $g_\parallel$ for the defect becomes $g_e+\frac{8}{3}P\Delta g_\perp$. Since $g_\parallel$ is at most 2.0031 (see Sec. III), P is less than 2.5%. This effect then could reduce the value of b_2 by about 7% at most; the very small experimental value still remains unexplained.

b. Case of a hybridized orbital. We have so far assumed that the unpaired electron occupies a pure p orbital possessing inversion symmetry; however, this is not required by the symmetry of the defect. Because the O^- ion site lacks inversion symmetry, the real hole orbital could be better represented by a hybridized s-p orbital directed towards the vacancy. Hybridization would displace the center of gravity of the electronic charge distribution along the $\vec{c}$ axis. It would therefore modify the value of b for the axial nucleus without markedly changing it for the laterally situated nuclei 1 and 3 (the b' parameters for the latter nuclei would be modified, but only in the case of strong hybridization). We will attempt to estimate the possible extent of this effect by considering a mixing of the ground state configuration $C_0=1s^2 2s^2 2p^5$ with the excited-state configuration $C_1=1s^2 2s^1 2p^6$, neglecting contributions from other configurations.

The problem of calculating the parameters b and b' reduces to a monoelectronic calculation for the wave function of the unpaired electron:

$$\phi = n|2p_z\rangle + m|2s\rangle.$$

For the parameters b and b' of a given nucleus, we now obtain

$$b = g_e g_n \mu_B \mu_N [1/v^3 + (2\sqrt{3}\, n\cos\tau/v^4) m\rho_{2s;2p} + \tfrac{6}{5} n^2 (3\cos^2\tau - 1)\langle\rho^2\rangle/v^5], \quad (11)$$

$$b' = g_e g_n \mu_B \mu_N \tfrac{3}{5} \sin^2\tau (\langle\rho^2\rangle/v^5) n^2. \quad (12)$$

Here, v and τ are as defined previously: we continue to assume that the principal axis z of the hyperfine interaction is parallel to the O^--nucleus–Be^{2+}-nucleus direction. The quantity $\rho_{2s;2p}$ is defined by the integral $\int_0^\infty R_{2s}(\rho)R_{2p}(\rho)\rho^3\, d\rho$, where $R_{2s}(\rho)$ and $R_{2p}(\rho)$ are the radial parts of the orbitals $2s$ and $2p$. The mixing coefficient m is given by $m=\langle C_0|V_C|C_1\rangle/(E_1-E_0)$, where E_1-E_0 is the energy difference between the excited- and ground-state configurations. Only the linear part of the crystal-field Hamiltonian V_C enters in the calculation of the mixing coefficient; if we include only the contribution of the three nearest-neighbor Be^{2+} ions, this term is

$$V_C^{(1)}(\vec{r}) = -e[(3q_{Be^{2+}}/v_1^2)\cos\tau_1]\, r\cos\theta,$$

where $\vec{r}$ defines the position of the electron with respect to the O^- ion nucleus.

We then obtain

$$b = g_e g_n \mu_B \mu_N [1/v^3 - (12n/v^4)\cos\tau(e^2/v_1^2)\cos\tau_1 \times (\rho_{2s;2p})^2/(E_1-E_0) + \tfrac{6}{5} n^2 (3\cos^2\tau - 1)\langle\rho^2\rangle/v^5]. \quad (13)$$

The energy of the excited configuration C_1 is not known exactly. The value 120 000 cm^{-1} has been proposed[23] as an extrapolation from the spectroscopic data for the isoelectronic series FI, NeII, ..., given in Moore's tables.[24] From the Hartree-Fock form of the $2s$ orbitals in O^-,[20] we calculate the value 0.652 Å for $\rho_{2s;2p}$. In Table II, we give the resultant values of the mixing coefficient squared m^2 for several values of the angle τ_1 and a fixed distance $v_1=1.70$ Å. We see that the anticipated degree of hybridization is small, even for the highest angles.

If we take $\tau_1=102°$, the hybridization reduces the interaction b_2 with the axial nucleus to 764 kHz,

TABLE II. Square of the mixing coefficient m of the orbital $2s$ hybridised with the orbital $2p$ as a function of the angle τ_1 between the axis of the $2p$ orbital ($\vec{c}$ axis) and the O^--Be^{2+} direction.

τ_1	90°	95°	100°	102°	105°	109.5°
m^2	0	0.004	0.017	0.024	0.039	0.063

which is closer than the value 970 kHz deduced for the case of a pure p orbital to the experimental value 595 kHz. However, part of the improved agreement comes from the fact that increasing the angle of the bonds with the first neighbors increases the distance between the O^- ion and nucleus 2 to $v_2 = 2.55$ Å.

For the nearest-neighbor nucleus 1, this degree of hybridization has only a small effect on the results previously obtained. We find now that $v_1 = 1.70$ Å and $\langle\rho^2\rangle = 0.73$ Å^2 (instead of $v_1 = 1.72$ Å and $\langle\rho^2\rangle = 0.75$ Å^2). For the lateral nnn nucleus 3 (now situated at angle $\tau_3 = 96.5°$), the previous results are not modified: $v_3 = 3.15$ Å and $b_3' = 16$ kHz.

Given these results, one might attempt to reduce the residual disagreement for the axial nucleus by increasing the degree of hybridization. However, a consideration of the effect this would have on the orientations of the principal hyperfine axes for the lateral nuclei 1 and 3 prevents us from doing this. Up till now, we have assumed that the principal hyperfine axis coincides with the O^- nucleus $-Be^{2+}$ nucleus direction exactly. We will now reexamine this point.

A tedious but straightforward calculation shows that the nondiagonal term B_{xz} of the hyperfine tensor is proportional to the quantity

$$(1/v^2)\{0.5\sin 2\alpha + (n^2\langle\rho^2\rangle/v^2)[0.25\sin 2\alpha - 0.8\sin 2\beta + 1.75\sin 2\alpha\cos(2\alpha - 2\beta)] + (2nm\rho_{2s;2p}/\sqrt{3}\,v) \times [2.5\sin 2\alpha\cos(\alpha - \beta) - \sin(\alpha + \beta)]\},$$

where β is the angle $\geq 90°$ between the axis of the orbital ($\vec{c}$ axis) and the principal axis z, and α is the angle between the O^--nucleus $-Be^{2+}$-nucleus direction and the z axis (the latter angle is taken positive if this direction lies between the $\vec{c}$ axis and z).

For the case of a pure p orbital ($n = 1, m = 0$), this expression shows that the hyperfine axis z will be inclined at an angle β which is smaller than the internuclear angle τ, because it is closer to one lobe of the p orbital, which we will call the "lower" lobe, than to the other. This effect increases with $\langle\rho^2\rangle$ and with τ; thus, it will increase if the angle τ is increased in order to attempt to increase the degree of hybridization. It is opposed by the contrary effect of the hybridization with $2s$, which removes electronic charge to the "upper" lobe. The first effect dominates in determining the orientation β of the z axis for the nearest-neighbor nucleus but it decreases very rapdily with distance. We thus obtain the following results:

Taking $\tau_1 = 102°$, we calculate that the hyperfine axis for the nearest-neighbor nucleus makes an angle $\beta_1 = 100°$ with the $\vec{c}$ axis; this is greater than the experimental value 98.5°. On the other hand, for nucleus 3, the value then calculated for β, namely $\beta_3 = 98°$, is then greater than the internuclear angle $\tau_3 = 96.5°$ and greater than the experimental value $\beta_3 = 95°$.

Thus, even if we found some way of increasing the hybridization without correlatively bringing the O^- ion closer to the vacancy, that is without increasing the angle τ_3, the angle β_3 would still increase simply by the effect of the hybridization and the disagreement between the calculated and measured values of β_3 would increase further.

We therefore require another mechanism which reduces b_2 but which has an opposite effect on the angle β_1 and β_3 of the hyperfine axis compared with the above effect of the hybridization.

c. Spin transfer to neighboring anions by overlap. The mechanism which we invoke is the partial transfer of the unpaired spin to the three O^{2-} ions which are common to the nearest-neighbor Be^{2+} ions and the axial nnn Be^{2+} ion. This transfer results from the overlap of the $2p_z$ orbital on the O^- ion and the occupied orbitals on the O^{2-} ions. Its effect is greater than that of the direct overlap between the $2p_z$ orbital and the $1s$ orbital of the axial Be^{2+} ion (discussed earlier) because the O^{2-} ions have considerable spatial extension in the crystal.

We will not discuss this process quantitatively. We simply note that a partial delocalization of the unpaired electron onto the three "lateral" nearest O^{2-} neighbors of the axial beryllium would produce a considerable reduction of the calculated anisotropy constant b_2. A very rough calculation, in which we suppose the transferred spin densities to be concentrated on the nuclei of the O^{2-} ions, shows that a total transfer of about 10% would reduce b_2 by about 190 kHz, giving agreement between the calculated and experimental values.

Another effect of this spin delocalization would be to reduce the angle β of the hyperfine axes. This also goes in the right direction to make the calculated and experimental values agree.

Thus, a combination of the effects of hybridization and delocalization can explain the value of the

parameter b_2 without changing the principle of an outward relaxation of the O^- ion away from the vacancy.

2. Discussion of contact interactions

There are three mechanisms which can produce an isotropic hyperfine interaction with a nucleus situated in the neighborhood of a paramagnetic defect. They are the overlap of orbitals on different centers, covalence, and exchange polarization. The former two produce a positive spin density and the latter mechanism a negative spin density at the nucleus.

For the first-neighbor nuclei, since the theory of Sec. IV B 1 requires b to be negative, the parameter a is positive, that is, the spin density is negative. We can compare this result with that obtained by Gazzinelli and Mieher[25] for the V_k center in LiF (an F_2^- molecular ion occupying a pair of anion sites). These authors found negative spin densities at the nuclei of the Li^+ and F^- ligands lying in the nodal plane of the defect. In order to interpret this result, Ikenberry *et al.*[26] calculated the contribution due to exchange polarization of the core electrons (1s for Li^+, 1s and 2s for F^-). Their calculated contact interactions $a(^7\mathrm{Li}) = -5.03$ MHz and $a(^{19}\mathrm{F}) = -6.60$ MHz are in good agreement with the experimental values −4.12 and −6.69 MHz, respectively. They found that the indirect polarization effect, involving the core electrons of the F_2^- molecular ion itself, is negligible: the predominant term is the direct exchange interaction between the ligand and the unpaired F_2^- orbital.

For the V^- center in BeO, one can interpret the contact interaction with the first-neighbor beryllium nuclei along the same lines. The observed negative spin density comes from the polarization of the 1s core of the Be^{2+} by direct interaction with the valence orbital of the O^- ion. This analogy between the V^- center and the V_k center appears justified for the following reasons: The unpaired electron orbital of the V^- center is mainly pure p type and, with the effect of the distortion, the first neighbors lie almost in the plane of this orbital. By comparison, in the V_k center, the unpaired electron occupies a σ_u molecular orbital, which is antisymmetric with respect to a reflection in the nodal plane and which can be considered in a simple model[27] to be a linear combination of the p orbitals on the two anions.

For the next-nearest-neighbor nucleus lying on the symmetry axis of the defect, the value of a is much smaller than for the nn nuclei and is negative, $a = -282$ kHz. The covalency mechanism should not be strongly involved in producing this positive spin density since this beryllium ion is not directly linked to the O^- ion. We therefore must consider the overlap and exchange polarization mechanisms.

A recent study by Schirmer[28] of the isotropic hyperfine constants at the lithium nucleus in the V_{Li} center (hole trapped at a substitutional Li^+) in BeO, ZnO, MgO, and CaO indicates that these two mechanisms can explain the spin densities observed in that case, providing that one allows for the overlap with the O^{2-} ions surrounding the Li^+ ion. This overlap tends to reduce greatly the positive contribution to the spin density due to overlap between the orbitals of the O^- and Li^+ ions. The final result in the V_{Li} center is a negative spin density at the lithium nucleus, owing to the dominant contribution of the direct exchange polarization.

It would seem that in our case the role of the overlap with the O^{2-} ions surrounding the nucleus in question is more important than in the problem considered by Schirmer. With the effect of the distortion, the O^- ion is at similar distance from the nucleus (2.50 Å in the V^- center, 2.20 Å in the V_{Li} center in MgO). It is probably closer to the O^{2-} ions which surround the nucleus. Also, these anions make up a plane lying between the O^- ion and the Be^{2+} ion. Thus the geometry of the BeO center must increase the importance of the indirect mechanisms. The measured value for the isotropic interaction with the axial nnn beryllium nucleus is small, which indicates that there is a near cancellation of the different mechanisms.

The lateral nnn nuclei are further away from the O^- site than the nucleus just considered (3.15 Å instead of about 2.50 Å). Moreover, these nuclei lie almost in the nodal plane of the unpaired p electron of the O^- ion. One would thus expect that the isotropic interaction would be very small, in agreement with experiment, which gives $a = 0.004 \pm 0.004$ MHz.

3. Theory of g factors

In the model proposed for the V^- center, the principal values of the $\vec{\vec{g}}$ tensors are those of the ground state of the O^- ion in the crystal field:

$$g_\parallel = g_e = 2.0023, \quad g_\perp = g_e - 2\lambda n^2/\Delta E. \tag{14}$$

The expression for $g_\perp$ differs from that given in Sec. III in that it contains n, the coefficient describing the proportion of 2p orbital in the wavefunction of the unpaired electron.

The experimental value of $g_\parallel = 2.0026 \pm 0.005$ is in good agreement with this model. Using the experimental value of $g_\perp$, the value $\lambda = -135$ cm^{-1} estimated by Bartram *et al.*[29] by extrapolation of experimental values for the isoelectronic series $Si^{5+}, \ldots, F^0, \ldots$ and the value 0.99 for n given by the discussion of Sec. IV B 1, we calculate ΔE

$= 20.5 \times 10^3$ cm^{-1}.

One can deduce a theoretical value for the energy difference ΔE between the ground and excited states in a very simple model which allows only for the crystal field produced by the nearest neighbors of the O^- ion, which are considered as point charges $+2|e|$. The unpaired electron is assumed to occupy a pure p orbital in the O^- ion. This model predicts

$$\Delta E = \tfrac{9}{5}\langle \rho^2 \rangle (e^2/v_1^3)(3\cos^2\tau_1 - 1). \quad (15)$$

Using the previously determined values for v_1, τ_1, and $\langle \rho^2 \rangle$ [Sec. IV B 1], we calculate $\Delta E = 26.5 \times 10^3$ cm^{-1}. This value is somewhat larger than that deduced from the experimental value of $g_\perp$. Part of the disagreement could be explained by the fact that the spin-orbit coupling in the O^- ion in the crystal should be increased with respect to that of the free ion, owing to the contraction of the $2p$ orbital mentioned earlier.

Thus, the simple crystal-field theory appears to give a good description of the principal values of the $\vec{\vec{g}}$ tensor for the V^- center in BeO. However, this result may be fortuitous, given the problems encountered in explaining the g values in the case of the similar centers in the other alkaline earth oxides.[30]

V. NONAXIAL V^- CENTER

Our study of the nonaxial configuration of the V^- center has been less detailed than that of the axial configuration. Because it has lower symmetry (C_s symmetry), the nonaxial defect has six different sites, which produces difficulties in the experimental ENDOR measurements and their analysis: the ENDOR lines are less intense (since the ESR lines are less intense) and there is a mixture of different ENDOR spectra, since it is hard to avoid simultaneous saturation of the ESR lines of the different sites.

Figure 13(a) shows the ENDOR spectrum which is obtained by saturating the ESR line of the nonaxial defect when $\vec{H}_0$ is parallel to $\vec{c}$. We have obtained several angular variations of the nearest-neighbor ENDOR lines while saturating the ESR lines corresponding to different sites. Figure 14 shows the variation obtained by rotating $\vec{H}_0$ in a $(1\bar{2}10)$ plane while saturating the highest-field ESR line (see Fig. 2). The ENDOR results show that the defect has very accurately C_s symmetry. For a given site, there exist two types of nearest neighbors. One type consists of a single nucleus, which lies in the symmetry plane of the defect. The other type consists of two equivalent nuclei placed symmetrically with respect to this plane and lying in the same (0001) plane as the cation vacancy. For the latter nuclei, we have only

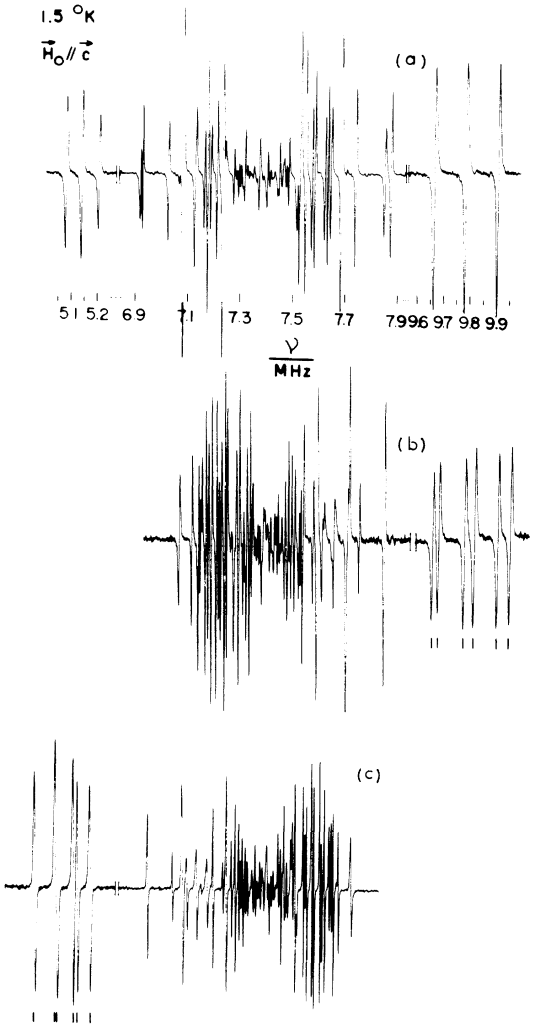

FIG. 13. (a) 1.5 °K ENDOR spectrum of the nonaxial V^- center for $\vec{H}_0$ parallel to $\vec{c}$. (b) High-frequency part of the ENDOR spectrum of the V^0 center obtained while saturating the $+1 \longleftrightarrow 0$ ESR line and (c) low-frequency part of the V^0 center's spectrum while saturating the $0 \longleftrightarrow -1$ ESR line.

analyzed the experimental results approximately, but we can state that they have very similar hyperfine interactions to the first mentioned nucleus. The hyperfine parameters determined for this nucleus lying in the symmetry plane are given in Table III.

From the results obtained for this nucleus, it appears that the magnetic interaction with the nearest-neighbor nuclei in the nonaxial defect has approximately cylindrical symmetry around an axis making an angle 98° with the principal axis of the $\vec{\vec{g}}$ tensor (which itself coincides very closely with the direction of the nonaxial Be-O bond in the perfect crystal). The relative geometric ar-

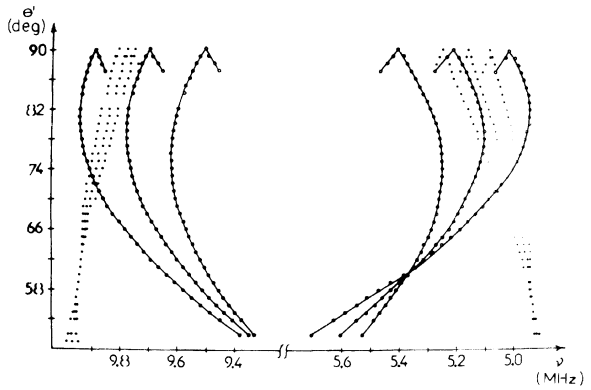

FIG. 14. Variation of the position of certain ENDOR lines of the nonaxial V^- center when $\vec{H}_0$ rotates in the $(1\bar{2}10)$ plane, making an angle θ' with $\vec{c}$. The curves correspond to the nearest-neighbor nucleus situated in the particular symmetry plane $(1\bar{2}10)$ of the defect.

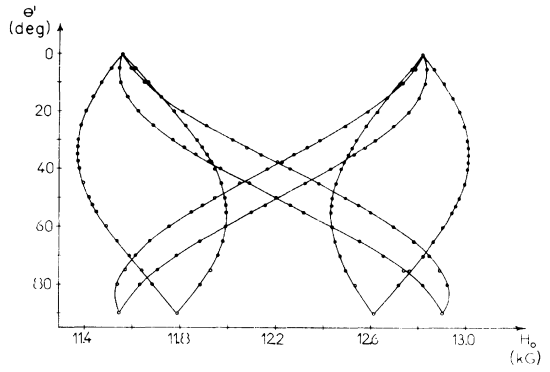

FIG. 15. Variation of the ESR lines of the V^0 center when $\vec{H}_0$ rotates in a $(1\bar{2}10)$ plane, making an angle θ' with the $\vec{c}$ axis.

rangement of the axes of the tensors $\vec{\vec{g}}$ and $\vec{\vec{A}}$ and the principal values of these two tensors are practically identical in the axial and nonaxial V^- centers. This confirms the similarity between the two configurations of the defect. The ENDOR observations also provide evidence for the close relation between the nonaxial V^- center and the center with spin $S=1$ which will be described in the following Sec. VI.

VI. V^0 CENTER

In addition to the spectrum of the V^- center, the low-temperature ESR spectrum of fast-particle-irradiated BeO crystals contains anisotropic lines corresponding to a center with spin $S=1$. We have previously attributed this spectrum to the neutral charge state of the beryllium vacancy, or V^0 center.[15]

The line positions were measured for $\vec{H}_0$ rotating in the $(1\bar{2}10)$ plane and in a (0001) plane (see Figs. 15 and 16). (The spectrum for $\vec{H}_0$ parallel to $\vec{c}$ was published in Ref. 15). These variations correspond accurately to a $S=1$ spin Hamiltonian:

$$\mathcal{H} = \mu_B(g_{xx}H_x + g_{yy}H_y + g_{zz}H_z) + D[S_z^2 - \tfrac{1}{3}S(S+1)] + E(S_x^2 - S_y^2), \quad (16)$$

where the parameters are measured to be

$$g_{xx} = 2.0107 \pm 0.0010, \quad D/h = -2900 \pm 30 \text{ MHz},$$
$$g_{yy} = 2.0154 \pm 0.0010,$$
$$g_{zz} = 2.0075 \pm 0.0010, \quad E/h = -560 \pm 6 \text{ MHz}.$$

The z axis is parallel to a $\langle 1\bar{2}10\rangle$ direction, which is the direction joining nearest-neighbor oxygens in the basal plane. The y axis lies in the $(1\bar{2}10)$ symmetry plane of the defect and makes an angle $34.3°$ with the $\vec{c}$ axis. The absolute sign of the constant D was determined from the relative intensities of the lines of the 1.5 °K spectrum.

The defect can be considered to be made up of two O^- ions situated in the base of the tetrahedron of anions containing a cation vacancy. In the two O^- ions, the unpaired electrons occupy p orbitals pointing towards the vacancy. A spin Hamiltonian having the form (16) can be deduced from the Hamiltonian for two O^- ions α and β:

$$\mathcal{H} = \mu_B\vec{H}_0\tfrac{1}{2}(\vec{\vec{g}}_\alpha + \vec{\vec{g}}_\beta)(\vec{S}_\alpha + \vec{S}_\beta) + \mu_B\vec{H}_0\tfrac{1}{2}(\vec{\vec{g}}_\alpha - \vec{\vec{g}}_\beta)(\vec{S}_\alpha - \vec{S}_\beta) + \mathcal{H}_{dip}(\vec{S}_\alpha, \vec{S}_\beta) + J\vec{S}_\alpha \cdot \vec{S}_\beta, \quad (17)$$

where S_α and S_β are equal to $\frac{1}{2}$. The first two terms represent the Zeeman interactions of the α and β O^- ions in the applied field; the third term is the dipolar magnetic interaction between these two ions; the fourth term is their isotropic exchange interaction.

TABLE III. Hyperfine constants (unit: MHz) for the beryllium nucleus which is a nearest neighbor of the O^- ion in the V^- center and is situated in the symmetry plane of the defect.

A_z/h	A_x/h	A_y/h	$Q_{z'}/h$	$Q_{x'}/h$	$Q_{y'}/h$	τ	τ'
+0.297	+4.655	+5.042	−0.083	+0.066	+0.017	11.5°	−6°
±0.006	±0.003	±0.003	±0.002	±0.001	±0.001	±0.5°	±0.5°

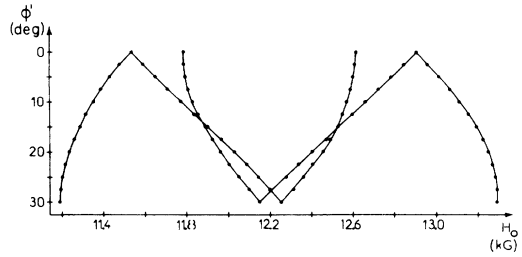

FIG. 16. Variation of the positions of the ESR lines of the V^0 center when $\vec{H}_0$ rotates in the (0001) plane, making an angle ϕ' with a $\langle 0\bar{1}10\rangle$ direction.

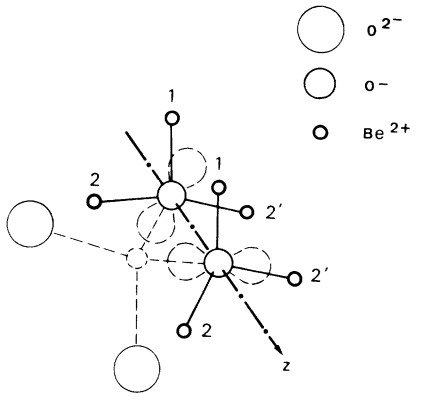

FIG. 17. Model of the V^0 center, showing the orientation of the two orbitals occupied by the holes and the disposition of the nearest-neighbor beryllium nuclei 1, 2, and 2'.

The nondiagonal second term of Hamiltonian (17) is certainly very small compared to the singlet-triplet separation. Thus the Hamiltonian of the triplet state reduces to

$$\mathcal{H} = \mu_B \vec{H}_0 \cdot \vec{\vec{g}} \cdot \vec{S} + \mathcal{H}_{dip}(\vec{S}), \qquad (18)$$

where $\vec{\vec{g}} = \frac{1}{2}(\vec{\vec{g}}_\alpha + \vec{\vec{g}}_\beta)$ and the second term has the form $\vec{S} \cdot \vec{\vec{D}} \cdot \vec{S}$.

From the proposed model and the ESR parameters of the nonaxial V^- center (Sec. III), one can make the following predictions concerning the $\vec{\vec{g}}$ tensor and fine-structure tensor $\vec{\vec{D}}$ of the $S=1$ center. First, $\vec{\vec{g}}$ and $\vec{\vec{D}}$ should have identical principal directions. In particular, their y axis should be perpendicular to the plane defined by the axes of the p orbitals occupied by the holes, which are shown in Fig. 17; therefore, they should lie in the $(1\bar{2}10)$ plane and make an angle of 34° with the $\vec{c}$ axis. Second, if one neglects the perturbing effect of each O^- ion on the other, the values of g predicted for the spin-1 center are $g_{xx} = 2.0120 \pm 0.0005$, $g_{yy} = 2.0164 \pm 0.0005$, and $g_{zz} = 2.0070 \pm 0.0005$. There is excellent agreement between these predictions and the experimental results given earlier.

The model also predicts that the fine-structure constants D and E should be negative, as observed. If the two O^- ions are approximated by point dipoles (in which case E would be zero), the measured value of D corresponds to a separation of 2.99 Å between the two O^- ions. This distance is slightly greater than the distance 2.71 Å between two anion sites in the perfect lattice, probably indicating a relaxation of the two O^- ions along the O^--vacancy directions.

Although the axial site is preferentially occupied in the case of the V^- center, we have not observed ESR spectra which could correspond to V^0 centers having one of the two holes trapped on the anion lying along the $\vec{c}$ axis from the vacancy.

Approximate measurements showed that the relative intensities of the ESR lines at 1.5 and 4.2 °K behave as if the triplet is the ground state. Or, if it is not, it cannot lie at more than 5 °K above the singlet. More precise measurements[31] have shown that if J is negative, $|J|$ is at most 1.5 °K. Since such a small singlet-triplet splitting appears very improbable, it is likely that the triplet is the ground state, with $|J|$ unknown.

V^0 type centers have been identified in three cubic alkaline earth oxides MgO,[1] CaO,[32] and SrO,[33] as well as in ZnO.[34] Analogous centers (in that case V^- centers) have been studied in Al_2O_3,[35] where the applicability of the model of a pair of O^- ions has been verified by the observation of the hyperfine interactions with the oxygen nuclei in a crystal enriched to 10% in ^{17}O.[36] In our case, additional evidence supporting the model comes from ENDOR observations of the ^9Be hyperfine interactions. To describe hyperfine interactions with nuclei of spin I, we must add to the Hamiltonian (17) a term

$$\vec{I} \cdot (\vec{\vec{A}}_\alpha \vec{S}_\alpha + \vec{\vec{A}}_\beta \vec{S}_\beta) = \vec{I} \cdot \tfrac{1}{2}(\vec{\vec{A}}_\alpha + \vec{\vec{A}}_\beta) \cdot (\vec{S}_\alpha + \vec{S}_\beta) + \vec{I} \cdot \tfrac{1}{2}(\vec{\vec{A}}_\alpha + \vec{\vec{A}}_\beta)(\vec{S}_\alpha - \vec{S}_\beta).$$

Within the triplet state, this reduces to the form $\vec{I} \cdot \vec{\vec{A}} \cdot \vec{S}$, where $\vec{\vec{A}} = \frac{1}{2}(\vec{\vec{A}}_\alpha + \vec{\vec{A}}_\beta)$. If the nucleus I is a nearest neighbor of ion α, the term $\vec{\vec{A}}_\beta$ is negligible, and we have

$$\vec{\vec{A}} = \tfrac{1}{2}\vec{\vec{A}}_\alpha. \qquad (19)$$

Thus, for such nuclei, the hyperfine interaction tensor should be approximately half that determined in the case of the nonaxial V^- center.

Figure 13 compares the ENDOR spectra (b) and (c) of the $S=1$ center with the ENDOR spectrum (a) of the nonaxial V^- center. The magnetic field $\vec{H}_0$ is parallel to $\vec{c}$. Spectrum (b) is obtained while saturating the $M_s = +1 \leftrightarrow M_s = 0$ transition of

the $S=1$ center, while spectrum (c) the $M_s=0 \rightarrow M_s=-1$. The outer lines of spectra (b) and (c) are attributable to two slightly inequivalent groups of nuclei 2 and 2′ which are nearest neighbors of the O^- ions and situated in the same (0001) plane as the cation vacancy (see Fig. 17). In the V^- center, nuclei 2 and 2′ are equivalent first neighbors of the single O^- ion and give a single set of ENDOR lines, the outer triplets in spectrum (a) with respect to the resonance frequency of the free beryllium nucleus, the central lines of the various quadrupole triplets lie at the following positions: (a) in the high-frequency spectrum: +2.384 MHz for the V^- center; +2.380 and +2.416 MHz for the V^0 center; (b) in the low-frequency spectrum: −2.243 MHz for the V^- center; −2.232 and −2.295 MHz for the V^0 center. Thus, for the two types of nuclei 2 and 2′, the agreement with the predictions of Eq. (19) is very good. This agreement has also been verified for other orientations of the magnetic fields.

In addition, from the ENDOR line positions, one can determine the signs of the components of the $\vec{\vec{A}}$ tensor, which turn out to be positive, as was required by the theory of Sec. IV B 1.

The slight difference between the two types of nuclei 2 and 2′ arises from two main causes. First, the electrostatic environment of the α O^- ion is perturbed by the presence of the β O^- ion on the neighboring anion site; this modifies the orbital occupied by the hole and differentiates the two types of nuclei. Second, we have neglected the contribution of the term $\vec{I}\cdot\vec{\vec{A}}_\beta\cdot\vec{S}_\beta$ which represents the magnetic interaction of the first neighbors of the α O^- ion with the β O^- ion. This interaction is different for the two nuclei 2 and 2′.

In summary, these measurements provide an excellent confirmation of the proposed model: the V^0 center is made up of two exchange-coupled O^- ions situated next to a cation vacancy. The exchange is probably ferromagnetic. The ions are separated by about 3 Å and do not form an O_2^{2-} molecular ion placed in the crystal.

VII. V_B CENTER

After an ionizing irradiation with γ rays, our as-received BeO crystals give ESR spectra at room temperature which appear very similar in their g factors and their hyperfine structure to the spectra given by the V^- center at helium temperature. These spectra have been attributed to a V^- center associated with a trivalent impurity, probably B^{3+}, which occupies a nearby cation site.[14a,18] The idea of the presence of an impurity ion was used to explain the stabilization of the hole on a single oxygen at room temperature. Two types of spectra can be distinguished, which we will call (loosely) "axial," where the axis of the $\vec{\vec{g}}$ tensor is approximately along $\vec{c}$ and "nonaxial," where the $\vec{\vec{g}}$ tensor axis is inclined at 109° to $\vec{c}$.

The ENDOR spectrum shown in Fig. 18 corresponds to the nonaxial defect. It is centered on the resonance frequency of the isotope ^{11}B ($I=\frac{5}{2}$, 80.4% natural abundance) in the applied field $\vec{H}_0$, which therefore establishes that boron is the trivalent impurity associated with the defect. The complexity of the spectrum, even when $\vec{H}_0$ is parallel to $\vec{c}$, shows that several distinct configurations of the vacancy-impurity complex are pres-

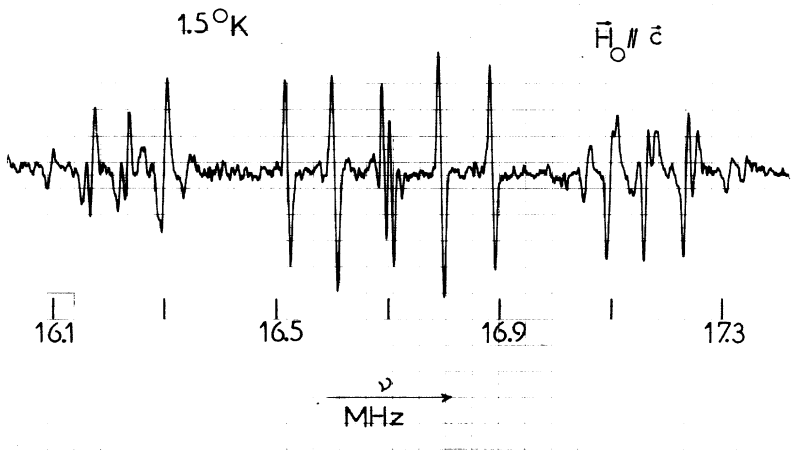

FIG. 18. 1.5 °K ENDOR spectrum of the nonaxial V_B center for $\vec{H}_0$ parallel to $\vec{c}$ showing the lines corresponding to transitions of ^{11}B nuclei in the vicinity of the cation vacancy.

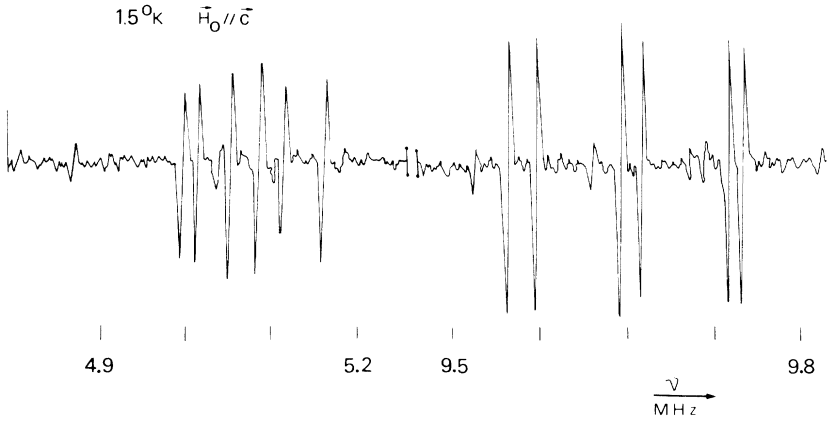

FIG. 19. 1.5 °K ENDOR spectrum of the nonaxial V_B center showing the transitions of the next-nearest-neighbor beryllium nucleus situated in the plane of approximate symmetry of the defect.

ent in the crystal. It appears probable that the most stable configurations would be those in which the vacancy and the B^{3+} are nearest neighbors. For the nonaxial center, there exist two possible nonequivalent configurations of this type.

The central region of the spectrum, made up of two intense triplets centered at 16.5 and 16.9 MHz certainly corresponds to one of these configurations. We have attempted to identify which one, trying to determine the orientation of the $O^- - B^{3+}$ with respect to the $\vec{c}$ axis. This was not possible, however, because for $\vec{H}_0$ not parallel to $\vec{c}$, there are far too many ENDOR lines and the signal-noise ratio is poor.

Figure 19 shows the low- and high-frequency halves of the ^{9}Be ENDOR spectrum which is obtained by saturating the ESR line of the nonaxial V_B center when $\vec{H}_0$ is parallel to $\vec{c}$. For the corresponding nonaxial configuration of the V^- center, each of these two ENDOR regions consists simply of one quadrupole triplet, which is associated with two equivalent nearest-neighbor beryllium nuclei. In the present case, each triplet is split in two. If we assume that these beryllium ENDOR lines and the boron ENDOR lines discussed above belong to the same defect, we can attribute this doubling of the ENDOR lines to a symmetry lowering produced by the impurity: this renders the two nearest-neighbor beryllium nuclei inequivalent. However, this still does not enable us to identify the vacancy-impurity configuration in question. For both configurations in which the vacancy and the impurity are nearest neighbors, the impurity lies out of the plane defined by the $\vec{c}$ axis and the O^--vacancy direction, thus lowering the symmetry of the center to C_1.

The influence of the impurity on the ENDOR spectrum can be understood in the model of an O^- ion subjected to a crystal field. The diagonalization of the ^2P ground term will be modified under the perturbing action of the field of the impurity. That is, the axis of the p orbital occupied by the unpaired electron will change slightly, and this orbital will then appear different to the nuclei. A simple calculation shows that the rotation of the p orbital will be at most a few degrees, but this is enough to produce an observable splitting in the ENDOR spectra.

We have also established the presence of a boron impurity in the "axial" V_B center. The existence of B^{3+}-vacancy associates in our crystals is not surprising for in the γ-irradiated samples we have also detected the ESR spectra of isolated neutral boron donors.[37] The introduction of the donor impurity boron as B^{3+} ions may be compensated by the introduction of cation vacancies, in the ratio of one vacancy for each two B^{3+}. Presumably, a fraction of the boron impurities are present as isolated B^{3+} ions, while another fraction is associated with the cation vacancies to form an acceptor center.

We note also that the ENDOR spectrum of the axial V_B defect contains a quadrupole triplet centered exactly on the resonance frequency of the free ^{9}Be nucleus. This is shown in Fig. 20. We attribute the triplet to distant Be nuclei weakly coupled to the defect, that is, to nuclei for which

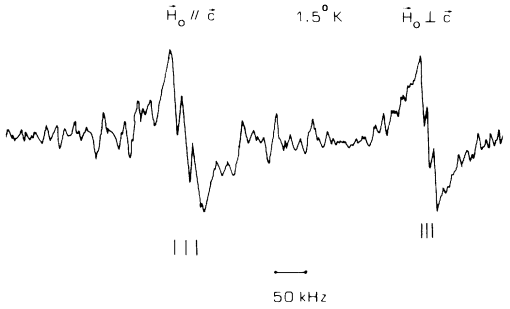

FIG. 20. 1.5 °K ENDOR spectrum of distant ^{9}Be nuclei in BeO as obtained by saturating the ESR line of the axial V_B center.

the interaction with the electronic spin density simply broadens the nuclear transistions. The splitting thus enables us to measure the axial quadrupole interaction between the quadrupole moment of the beryllium nucleus and the electric field gradient at this nucleus in the perfect crystal. We obtain $e^2qQ/h = 39 \pm 1$ kHz, which agrees well with the NMR measurements of Sholl and Walter[38] and Thorland *et al.*,[39] who found 38.4 ± 0.4 and 39.4 ± 0.2 kHz, respectively.

VIII. CONCLUSION

In fast-particle-irradiated crystals of BeO, we have identified two $S = \frac{1}{2}$ trapped hole centers, which constitute two slightly different configurations of the V^- center, that is the isolated cation vacancy with a trapped hole. In the axial configuration, the hole is localized on an oxygen situated along the $\vec{c}$ axis from the vacancy; in the nonaxial configuration, it is trapped on an oxygen situated in the base of the tetrahedron. We have measured the hyperfine interactions of the axial defect with three different shells of neighboring beryllium ions, using the ENDOR technique. The detailed analysis of the magnetic dipolar interaction with these nuclei enabled us to demonstrate the highly localized nature of the ground state of the defect and provided detailed information about its electronic structure. This analysis also enabled us to determine the geometric structure of the defect, giving the nature and magnitude of the distortions of the ion positions. The negative spin density observed at the nearest-neighbor beryllium nuclei was attributed to the direct exchange polarization of the ligands by the unpaired O^- orbital.

The neutral charge state of the vacancy (V^0 center) has also been observed in the fast-particle-irradiated crystals. A comparison of the ENDOR spectra of the V^0 center with those of the nonaxial V^- center confirmed the proposed model, namely a pair of O^- ions next to a cation vacancy.

Finally, we have shown that the as-received crystals contain associated defects consisting of a cation vacancy and a B^{3+} impurity. This defect, which can exist in several different configurations, traps a hole under gamma irradiation.

Owing to the various ENDOR results obtained, this work constitutes the most complete study performed up to the present time for the ground state of a V-type center in an oxide. It is to be hoped that in the near future measurements of the optical absorption will provide information about the excited states of this defect in BeO.

ACKNOWLEDGMENTS

We would like to thank Dr. R. T. Cox for many enriching discussions and for great help in the preparation of the manuscript. The assistance of Dr. G. Rius, Dr. C. Santier, and R. Picard in the construction of the ENDOR apparatus is gratefully acknowledged.

---

†Part of B. Maffeo's work submitted as a "Docteur d'Etat es Sciences" thesis, supported by the Brazilian agency CAPES and the French agency "Fondation Joliot-Curie."

*Present address: Departamento de Física, Pontifícia Universidade Católica do Rio de Janeiro, Rua Marquês de São Vicente, 209/225-Gâvea 20000 Rio de Janeiro, Brazil.

[1]J. E. Wertz, R. Auzins, J. H. E. Griffiths, and J. W. Orton, Discuss. Faraday Soc. 28, 136 (1959).

[2]B. Henderson and J. E. Wertz, Adv. Phys. 17, 749 (1968).

[3]A. E. Hughes and B. Henderson, in *Point Defects in Solids*, edited by J. H. Crawford, Jr. and L. N. Slifkin (Plenum, New York, 1972), Chap. 7.

[4]M. M. Abraham, Y. Chen, and W. P. Unruh, Phys. Rev. B 9, 1842 (1974).

[5]Y. Chen, M. M. Abraham, L. C. Templeton, and W. P. Unruh, Phys. Rev. B 11, 881 (1975).

[6]A. J. Tench and M. J. Duck, J. Phys. C 6, 1134 (1973).

[7]E. H. Izen, R. M. Mazo, and J. C. Kemp, J. Phys. Chem. Solids 34, 1431 (1973).

[8]O. F. Schirmer, P. Koidl, and H. G. Reik, Phys. Status Solidi B 62, 385 (1974).

[9]B. H. Rose and D. L. Cowan, Solid State Commun. 15, 775 (1974).

[10]G. Rius and A. Hervé, Solid State Commun. 15, 421 (1974).

[11]L. E. Halliburton, L. A. Kappers, D. L. Cowan, F. Dravnieks, and J. E. Wertz, Phys. Rev. Lett. 30, 607 (1974).

[12]A. Schoenberg, J. T. Suss, S. Szapiro, and Z. Luz, Phys. Rev. Lett. 27, 1641 (1971).

[13]L. E. Halliburton, D. L. Cowan, W. B. J. Blake, and J. E. Wertz, Phys. Rev. B 8, 1610 (1973).

[14](a) A. Hervé and B. Maffeo, Phys. Lett. A 32, 247 (1970); (b) B. Maffeo, A. Hervé, G. Rius, C. Santier, and R. Picard, Solid State Commun. 10, 1205 (1972).

[15]B. Maffeo, A. Hervé, and R. T. Cox, Solid State Commun. 8, 2169 (1970).

[16]C. Santier, French patent E.M. 7025132 (1970).

[17]R. C. DuVarney, A. K. Garrison, and R. H. Thorland, Phys. Rev. 188, 657 (1969).

[18]A. Hervé, C.E.A. report (1969) (unpublished).

[19]A. K. Garrison and R. C. DuVarney, Phys. Rev. B 7, 4689 (1973).

[20]E. Clementi, IBM J. Res. Dev. Suppl. 9, 2 (1965).

[21]F. Gourary and J. Adrian, Solid State Phys. 10, 127

(1960).
[22]O. F. Schirmer, J. Phys. Chem. Solids, 32, 499 (1971).
[23]R. Schnadt and J. Schneider, Phys. Kondens. Mater. 11, 19 (1970).
[24]C. E. Moore, Natl. Bur. Stand. Circular No. 467, Vol. I (U.S. GPO, Washington, D. C.).
[25]R. Gazzinelli and R. L. Mieher, Phys. Rev. Lett. 12, 644 (1964); and Phys. Rev. 175, 395 (1968).
[26]D. Ikenberry, A. N. Jette, and T. P. Das, Phys. Rev. B 1, 2785 (1970).
[27]C. P. Slichter, *Principles of Magnetic Resonance* (Harper and Row, New York, 1963), Chap. 7.
[28]O. F. Schirmer, J. Phys. C 6, 300 (1973).
[29]R. H. Bartram, C. E. Swenberg, and J. T. Fournier, Phys. Rev. 139, A941 (1965).
[30]M. M. Abraham, Y. Chen, J. T. Lewis, and F. A. Modine, Phys. Rev. B 7, 2732 (1963).
[31]R. T. Cox and G. Rius (unpublished).
[32]B. Henderson and A. C. Tomlinson, J. Phys. Chem. Solids 30, 1801 (1969).
[33]A. J. Tench and M. J. Duck, J. Phys. C 8, 257 (1975).
[34]D. Galland and A. Hervé, Phys. Lett. A 33, 1 (1970).
[35]R. T. Cox, Solid State Commun. 9, 1989 (1971).
[36]R. T. Cox, thesis (Grenoble, 1972) (unpublished).
[37]A. R. Reinberg, J. Chem. Phys. 41, 840 (1964).
[38]C. A. Sholl and J. A. Walter, J. Nucl. Mater. 2, 2301 (1969).
[39]R. H. Thorland, A. K. Garrison, and R. C. DuVarney, Phys. Rev. B 5, 784 (1972).